REPORT DOCUMENTATION PAGE

Form Approved
OMB No. 0704-0188

1. AGENCY USE ONLY *(Leave blank)*

2. REPORT DATE
June 1, 1994

3. REPORT TYPE AND DATES COVERED

4. TITLE AND SUBTITLE
Signal Processing for High-Performance Image Formation

5. FUNDING NUMBERS
DAALO3-91-G-0118

6. AUTHOR(S)
Arun S.Karalamangala (aka K. S. Arun)

7. PERFORMING ORGANIZATION NAME(S) AND ADDRESS(ES)
University of Illinois at Urbana-Champaign
Grants and Contracts Office
109 Coble Hall
801 S. Wright Street
Champaign, IL 61820-6242

8. PERFORMING ORGANIZATION REPORT NUMBER

9. SPONSORING/MONITORING AGENCY NAME(S) AND ADDRESS(ES)
U. S. Army Research Office
P. O. Box 12211
Research Triangle Park, NC 27709-2211

10. SPONSORING/MONITORING AGENCY REPORT NUMBER
ARO 28476.8-MA-SDI

11. SUPPLEMENTARY NOTES
The view, opinions and/or findings contained in this report are those of the author(s) and should not be construed as an official Department of the Army position, policy, or decision, unless so designated by other documentation.

12a. DISTRIBUTION/AVAILABILITY STATEMENT
Approved for public release; distribution unlimited.

12b. DISTRIBUTION CODE

13. ABSTRACT *(Maximum 200 words)*

This research program investigated signal processing problems encountered in high-resolution image formation. Reliable imaging of scenes with high resolution and high speed is an important and key part of any defense system. In some imaging systems, the image has to be constructed from linear measurements and convex constraints(such as upper and lower bounds on image sample magnitude, and support limits). We studied iterative, finite parameter reconstructions that lead to images that meet constraints, match the data to within a pre-specified tolerance, and come closest to a given nominal. We addressed three different aspects of signal/image reconstruction, namely,

1. Developing fast algorithms for high resolution signal/image reconstruction
2. Resolutions Analysis of signal reconstruction algorithms.
3. Numerical and computational aspects of signal reconstruction viz: stability and regularization

14. SUBJECT TERMS
signal/image reconstruction; signal reconstruction

15. NUMBER OF PAGES
30

16. PRICE CODE

17. SECURITY CLASSIFICATION OF REPORT	18. SECURITY CLASSIFICATION OF THIS PAGE	19. SECURITY CLASSIFICATION OF ABSTRACT	20. LIMITATION OF ABSTRACT
UNCLASSIFIED	UNCLASSIFIED	UNCLASSIFIED	UL

SIGNAL PROCESSING FOR HIGH-RESOLUTION IMAGE FORMATION

FINAL REPORT

Arun S. Karalamangala (aka K. S. Arun)

28 September, 1994

U. S. ARMY RESEARCH OFFICE

DAAL03-91-G-0118

University of Illinois

This research program investigated signal processing problems encountered in high-resolution image formation. Reliable imaging of scenes with high resolution and high speed is an important and key part of any defense system. In some imaging systems, the image has to be constructed from linear measurements and convex constraints (such as upper and lower bounds on image sample magnitude, and support limits). We studied iterative, finite parameter reconstructions that lead to images that meet the constraints, match the data to within a pre-specified tolerance, and come closest to a given nominal.

We addressed three different aspects of signal/image reconstruction, namely:

1. Developing fast algorithms for high resolution signal/image reconstruction.
2. Resolutions Analysis of signal reconstruction algorithms.
3. Numerical and computational aspects of signal reconstruction viz. stability and regularization.

Important results in each of the above three topics are summarized below.

Summary of Important Results

1. Fast Algorithms

The standard approach to the problem of image reconstruction from linear measurements and convex constraints has been an alternating projections onto convex sets (POCS) algorithm, studied by Youla and others. The approach suffers from slow (linear) convergence, high computational cost and non-unique limits. We have developed a quadratically convergent iterative algorithm (Newton algorithm) for this problem. Central to the Newton algorithm is the derivative of the nonlinear projection operator onto a convex set. We obtained a new general mathematical result for the existence and construction of the derivative of the projection operator for a class of convex sets. This result was then used to give the Newton algorithm for the signal recovery problem. A salient feature of the algorithm is the *quadratic rate* of convergence.

We also studied the implementation aspects of the algorithm and developed a *computation and memory efficient* implementation of the algorithm using conjugate-gradient iterations within each Newton iteration. A remarkable feature of the algorithm with this implementation, is that each iteration has similar computational complexity as an iteration of the POCS algorithm. The faster rate of convergence of the algorithm (as compared to POCS) thus enables us to compute high resolution reconstructions with fewer computations. The algorithm has been tested extensively on imaging examples and we have obtained extremely good performance. In many image formation schemes, 6 to 7 iterations seem to suffice, compared to the 100s of iterations required by classical methods such as POCS.

2. Resolution analysis

Resolution ability is the ability to reproduce fine details such as, narrow peaks or closely spaced peaks in a signal. The study of resolution is important, since understanding the relationship between resolution limits and the various components of a recovery problem and algorithm, could help us design better data acquisition schemes and algorithms.

The earliest definition of resolution limit is the *Rayleigh Resolution Limit.* This definition is based solely on the observed data and not on any recovery algorithm. The definition is acceptable when there is no processing of the data to recover or enhance the features based on exploiting prior information. The Rayleigh limit is thus a lower bound on the achievable resolution.

We find that where infinitely many noise-free measurements are available, the resolution achievable is in fact independent of the width of the sampling pulse and depends only the inter-sample distance. The Rayleigh limit, on the other hand, is dictated by the width of the sampling pulse. In the presence of observation noise, however, the notion of exact recovery has to be abandoned and a new measure of resolution is necessary. We define a new measure based on allowable levels of worst-case error, and find that the resolution limit depends on the method of regularization used in the recovery algorithm.

In the more practical situation in which only finitely many noisy observations are avail-

able, the worst-case error is unbounded and so we have to restrict the search to a smaller set of signals. In order to meaningfully describe resolution limits for the problem of signal recovery from finitely many noisy observations, we restrict the class of signals to the set of *bandlimited* and *essentially timelimited* signals, since it describes most signals encountered in practice. This set is characterized by the well known orthonormal family of functions called the *Prolate Spheroidal Wave Functions* and is known to be approximately finite dimensional, which enables us to seek reconstructions from a lower dimensional subspace of the space of bandlimited signals. Reduction in dimension causes an error in the reconstruction, which we call the *intrinsic error*. A second error is incurred while determining the parameters describing the lower dimensional reconstruction. The reconstruction error is then the sum of these two errors. We show that the worst-case values of these two errors can be pre-computed for each choice of reduced dimension. The error computation provides both an optimal choice of dimension and a precomputed bound on the resolution ability of the algorithm.

3. Numerical and Computational aspects:

Most reconstruction problems are ill-posed. Therefore, regularization is needed for an approximate but stable computation of the solution. The truncated SVD approach is popular method of regularization. The selection of the proper rank is the main problem in this technique. We have developed a new rank selection strategy based on a bound on the noise energy alone. In the absence of bounds on the signal energy we enforce our belief that the signal energy cannot be large, by introducing a penalty on the solution in the worst-case (min-max) analysis. The rank is selected so that the worst case error with a penalty on the solution norm is minimum. This method of regularization was tested in bandlimited extrapolation problems and it gave excellent results.

List of Publications

1. L. C. Potter and K. S. Arun, "An iterative least-squares solution to constrained inverse problems : Theory and applications," *IEEE Trans. Acoust., Speech & Signal Proc.* Under review.

2. S. Dharanipragada and K. S. Arun, "Signal reconstruction using time-bandwidth dimension,," *IEEE Trans. Sig. Proc.* Under review.

3. S. Dharanipragada and K. S. Arun, "Minimum square deviation tomographic reconstruction from few projections," *Proc. Fifth Annual IEEE Smposium on Computer-based Medical Systems*, pp. 190–197, June 1992.

4. S. Dharanipragada and K. S. Arun, "Resolution limits in reconstruction," *Proc. IEEE Digital Signal Processing Workshop*, pp. 6.2.1–2, September 1992.

5. S. Dharanipragada and K. S. Arun, "A newton algorithm for convex constrained signal recovery," *Proc. IEEE Intl. Conf. on Acoustics, Speech and Signal Processing, Minneapolis*, pp. III:595–598, April 1993.

6. S. Dharanipragada and K. S. Arun, "A quadratically convergent algorithm for convex constrained signal reconstruction," *IEEE Trans Sig. Proc.* Under review.

7. S. Dharanipragada and K. S. Arun, "Resolution limits in signal recovery," *submitted to IEEE Trans Sig. Proc.*

8. Bhaskar D. Rao and K. S. Arun, "Model based processing of signals: A state space approach," *Proc. of the IEEE*, pp. 283-309, February, 1992.

9. K. S. Arun and D. R. Wagner, "High speed digital filtering: Structures and finite wordlength effects," *Journal of VLSI Signal Processing,* Vol. 4, pp. 355-370, 1992

Scientific Personnel Supported by this Project:

Faculty Principal Investigator: K. S. Arun

Graduate Research Assistant: S. Dharanipragada (earned PhD in October 1994) .

Resolution Limits in Signal Recovery*

S. Dharanipragada† and K. S. Arun‡

September 27, 1994

Abstract

Resolution analysis for the problem of signal recovery from finitely many linear samples is the subject of this paper. The classical Rayleigh limit serves only as a lower bound on resolution since it does not assume any recovery strategy and is based only on observed data. We show that details finer than the Rayleigh limit can be recovered by simple linear processing that incorporates prior information. We first define a measure of resolution based on allowable levels of error that is more appropriate for current signal recovery strategies than the Rayleigh definition. In the practical situation in which only finitely many noisy observations are available, we have to restrict the class of signals in order to make the resolution measure meaningful. We consider the set of bandlimited and essentially timelimited signals since it describes most signals encountered in practice. For this set we show how to precompute resolution limits from knowledge of measurement functionals, signal-to-noise ratio, passband, energy concentration regions, energy concentration factor, and a prescribed level of error tolerance. In the process we also derive an algorithm for high resolution signal recovery. We illustrate the results with examples in one and two dimensions.

EDICS category: 2.5
Permission to publish abstract separately granted.
Please address all corresspondence to S. Dharanipragada.

*This work was partially supported by the SDIO/IST under contract DAAL03-91-G-0118 managed by the U.S. Army Research Office.

†S. Dharanipragada is with the Coordinated Science Laboratory, University of Illinois at Urbana-Champaign, 1308 W. Main St., Urbana, IL 61801. E-mail: satya@uicsltg.csl.uiuc.edu, tel: (217) 244-6384.

‡K. S. Arun is with the Department of Electrical Engineering and Computer Science, University of Michigan at Ann Arbor, Ann Arbor, MI 48109. E-mail: ksarun@eecs.umich.edu.

1 Introduction

The problem of recovering signals from linear measurements arises in many applications, and several algorithms, linear and nonlinear, have been developed and analyzed for this problem [1, 2, 3, 4, 5, 6, 7, 8, 9]. However, the fundamental question regarding the *resolution ability* of a recovery algorithm is often left unanswered. Resolution ability is the ability to reproduce fine details such as, narrow peaks or closely spaced peaks in a signal. The study of resolution is important; in many applications it is necessary for the reconstruction algorithm to have a certain minimum resolution in order to be effective. For example, consider the digital mammography application, where a 2-D X-ray profile is to be reconstructed from samples. With current sensor technology and physical limitations, the sampling operation amounts to 2D pulse sampling with pulse width (Δ) at least 50 microns and sample spacing (τ) at least 50 microns, which limits the "resolution" obtainable from a single exposure to 50 microns or larger, i.e., details in the image that are narrower than 50 microns cannot be reproduced. The integration with a pulse of width 50 microns causes smearing of finer details, and the sample spacing of 50 microns can cause us to miss these details altogether. However, early detection of breast carcinoma requires that features of width 25 microns be reproduced in the image. The grain size of an X-ray film is small enough for these features to appear in the more conventional analog X-ray photographs. To make digital mammography equally useful for diagnostic radiology, resolution of at least 25 microns is required. More generally, the study of resolution limits is important since, it could help us assess the effectiveness of a particular algorithm, and compare different algorithms in a rational manner. Moreover, understanding the relationship between resolution limits and the various components of a recovery problem and algorithm, could help us design better data acquisition schemes and algorithms.

The problem of resolution analysis is twofold: first, we need a meaningful measure of resolution ability, and second, we have to be able to analyze the performance of a reconstruction algorithm in terms of the defined resolution measure. The earliest definition of resolution limit is the *Rayleigh Resolution Limit.* It is defined as follows:

Definition 1.1 (Rayleigh Resolution Limit) [10] If two equally strong point sources (impulse intensities), δ or more apart, are reproduced as peaks with at least a 19% intensity dip, and if sources less than δ apart are not reproduced as well, the resolution limit is said to be δ. ■

Equivalently, the Rayleigh resolution limit is inversely proportional to the main lobe width

of the point spread function of the blurring (or sampling) kernel. This definition is based solely on the observed data and not on any recovery algorithm. The definition is acceptable when there is no processing of the data to recover or enhance the features based on exploiting prior information. The Rayleigh limit is thus a lower bound on the achievable resolution. We might be able to do better with clever signal processing that exploits prior information, but we should always be able to achieve at least as much resolution as specified by the Rayleigh limit.

We find that where infinitely many noise-free measurements are available, the resolution achievable is in fact independent of the width of the sampling pulse and depends only the inter-sample distance. The Rayleigh limit, on the other hand, is dictated by the width of the sampling pulse. In the presence of observation noise, however, the notion of exact recovery has to be abandoned and a new measure of resolution is necessary. We define a new measure based on allowable levels of worst-case error, and find that the resolution limit depends on the method of regularization used in the recovery algorithm.

In the more practical situation in which only finitely many noisy observations are available, the worst-case error is unbounded and so we have to restrict the search to a smaller set of signals. In studying the problem of resolution in signal recovery Root et al. [11], [12] recognized the need for finite-dimensional approximations to overcome instability. They introduce the concept of an *error number*, which is defined as the mean-squared error averaged by the dimension of the approximating subspace. As dimension increases, the "detail" in the estimate increases but so does the error number. The authors thus bring out the trade-off between the achievable level of detail (i.e., resolution) and the error in reconstruction. However they do not quantify resolution (detail) and fail to provide resolution bounds.

We appeal to the Fourier uncertainty principle to bring out the relationship between resolution (detail) and bandwidth. In this sense our is similar in spirit to the classical Rayleigh resolution limit, but is based on a prescribed tolerance of the *relative error*.

In order to meaningfully describe resolution limits for the problem of signal recovery from finitely many noisy observations, we restrict the class of signals to the set of *bandlimited* and *essentially timelimited* signals, since it describes most signals encountered in practice. This set is characterized by the well known orthonormal family of functions called the *Prolate Spheroidal Wave Functions* and is known to be approximately finite dimensional, which enables us to seek reconstructions from a lower dimensional subspace of the space of bandlimited signals. Reduction in dimension causes an error in the reconstruction, which we call the *intrinsic error*. A second error is incurred while determining the parameters

describing the lower dimensional reconstruction. The reconstruction error is then the sum of these two errors. We show that the worst-case values of these two errors can be precomputed for each choice of reduced dimension. The error computation provides both an optimal choice of dimension and a precomputed bound on the resolution ability of the algorithm.

This paper is organized as follows: In Section 2 we formulate the signal recovery problem in a vector space setting. In Section 3 we analyze the resolution limits for the ideal situation of infinitely many noise-free observations and describe the effects of noise and regularization. Based on the results obtained, we suggest a method for improving resolution in the mammography application. In Section 4, which is the bulk of the paper, we examine the practical situation of finitely many noisy observations for resolution limits. We demonstrate the results in one and two dimensional examples.

2 The Signal Recovery Problem

We consider the problem of reconstructing 1D continuous-index signals from discrete linear measurements. The results presented here can be easily generalized to multidimensional signals. We demonstrate the generalization by way of an example in Section 4.

Let $L_2(R)$ be the space of finite-energy continuous-index signals with the natural inner product defined by

$$\langle x, y \rangle_{L_2(R)} = \int_R x(t)\overline{y(t)}\, dt,$$

where the overbars denote complex conjugation. Let $\mathcal{B}_\delta$ be the subspace of all signals bandlimited to $P_\delta = [\frac{-\pi}{\delta}, \frac{\pi}{\delta}]$ and let B denote the orthogonal projection operator onto $\mathcal{B}_\delta$. In practical terms, B is simply a ideal bandpass filter with a passband $P_\delta = [\frac{-\pi}{\delta}, \frac{\pi}{\delta}]$. Let $X(\Omega)$ denote the continuous-time Fourier transform (CTFT) of $x(t)$,

$$X(\Omega) = \mathcal{F}\{x(t)\} = \int_{-\infty}^{\infty} x(t)e^{-j\Omega t}dt,$$

and

$$\mathcal{F}\{Bx(t)\} = \begin{cases} X(\Omega) & -\frac{\pi}{\delta} \leq \Omega \leq \frac{\pi}{\delta} \\ 0 & else \end{cases}.$$

We address the problem of recovering a signal from $\mathcal{B}_\delta$ by using discrete linear measurements. Every linear continuous measurement functional on $L_2(R)$ can be expressed as an

inner product with a measurement signal in $L_2(R)$ [13]. Let g_i be measurement signals giving measurements $y_d(i)$ as

$$y_d(i) = \langle x, g_i \rangle = \int_R x(t)\overline{g_i(t)}dt. \tag{1}$$

Let T be the linear bounded operator on $\mathcal{B}_\delta$ representing the measurement process. Then

$$Tx = y_d, \quad x \in \mathcal{B}_\delta, \tag{2}$$

where y_d is the vector of measurements. If the number of measurements, p, is finite, y_d lies in C^p, otherwise y_d lies in $l_2(Z)$, the space of finite-energy discrete-index signals with the inner product

$$\langle x_d, y_d \rangle_{l_2} = \sum_{n \in Z} x_d(n)\overline{y_d(n)}. \tag{3}$$

We will use the subscript 'd' to identify discrete-index signals, their transforms, and discrete-time frequency responses. Let $X_d \in L_2([-\pi, \pi])$ be the discrete time Fourier transform of $x_d \in l_2(Z)$,

$$X_d(\omega) = \sum_{n \in Z} x_d(n)e^{-j\omega n}, \quad \omega \in [-\pi, \pi].$$

Finally, the adjoint operator T^* maps a vector $v_d \in C^p$ or $l_2(Z)$ to a signal $T^*v_d = \sum_{\mathcal{M}} v_d(i)Bg_i$ in $\mathcal{B}_\delta$, a simple linear combination of the measurement signals. Here $\mathcal{M}$ denotes either the index set $\{1, 2, \cdots, p\}$ or Z.

In the ideal situation of accurate measurements, the problem of signal recovery from linear measurements is equivalent to that of finding a solution to the linear operator (2). However, in practice, the measurements are corrupted by noise. Let n_d denote the noise vector, then

$$z_d = Tx + n_d \tag{4}$$

and the signal recovery problem is that of reconstructing $x \in \mathcal{B}_\delta$ from z_d.

In the next section we consider the signal recovery problem where infinitely many measurements are available and examine the resolution limit of the minimum norm least squares solution to (2). We also describe the effects of noise on the resolution limit in this situation. The bulk of this paper, however, deals with resolution limits in the practical case of a finite number of noisy measurements, starting from Section 4

3 Resolution Limit with Infinitely Many Measurements

It is well known that if all signals bandlimited to $[-\frac{\pi}{\delta}, \frac{\pi}{\delta}]$ can be reconstructed perfectly, then two point sources spaced δ apart will show up as distinct peaks in the reconstruction.

This observation is a natural basis for our first definition of resolution.

Definition 3.1 (Resolution limit under ideal conditions) A reconstruction algorithm is said to have an *ideal resolution* of δ if signals bandlimited to $[-\frac{\pi}{\delta}, \frac{\pi}{\delta}]$ can be reconstructed perfectly under noise-free conditions. ■

This definition, unlike the Rayleigh definition, is based on the recovered signal instead of on the observed signal. Hence, the resolution limit will depend on the recovery strategy adopted. We will show next that we can do better than the Rayleigh resolution limit.

When (2) admits no exact solution because of noise in measurements, a popular recourse is to seek the unique minimum norm least squares solution of (2)

$$\hat{x}_{MNLS} = T^*(TT^*)^\dagger z_d, \tag{5}$$

where $(TT^*)^\dagger$ denotes the pseudoinverse of the composition TT^*. From the description of the measurement operator and its adjoint it follows that, for $v_d \in l_2(Z)$,

$$(TT^* v_d)(i) = \sum_{k \in \mathcal{Z}} z_d(k) \langle Bg_k, g_i \rangle_{L_2(R)}. \tag{6}$$

In many applications such as digital mammography and deconvolution, the measurement functions are uniformly translated versions of a basic sampling kernel/pulse g_0:

$$g_k(t) = g_0(t - k\tau), \ \ \tau > 0. \tag{7}$$

With this assumption, $\langle Bg_k, g_i \rangle_{L_2(R)} = \langle Bg_k, Bg_i \rangle_{L_2(R)}$ depends only on $i - k$ and not on absolute time, and, hence, TT^* is a convolution. The shift-invariant property of the sampling functions and the TT^* operator is exploited to obtain frequency domain expressions for T, T^*, TT^* and the MNLS solution next.

From (1) and (7) we obtain,

$$Y_d(\omega) = \sum_{k \in \mathcal{Z}} X(\frac{\omega - 2\pi k}{\tau}) \overline{G(\frac{\omega - 2\pi k}{\tau})}, \tag{8}$$

where $Y_d(\omega)$ is the DTFT of y_d and $X(\Omega)$ and $G(\Omega)$ are the CTFTs of x and g_0 respectively. If $\hat{x}(t) = T^* v_d$, then

$$\hat{x}(t) = (T^* v_d)(t) = \sum_{k \in \mathcal{Z}} v_d(k)(Bg_0)(t - k\tau) \tag{9}$$

which in the frequency domain is

$$\hat{X}(\Omega) = \Pi(\Omega) G(\Omega) V_d(\Omega\tau). \tag{10}$$

Here $\Pi(\Omega)$ is the frequency response of the ideal bandpass filter for passband $P_\delta = [\frac{-\pi}{\delta}, \frac{\pi}{\delta}]$, $\hat{X}(\Omega)$ is the CTFT of $\hat{x}$ and $V_d(\omega)$ is the DTFT of v_d. The TT^* operation is equivalent to discrete-time convolution with a kernel given by

$$h(k) = \langle Bg_k, Bg_0 \rangle_{L_2(R)} = \int_R g_0(t - k\tau)\overline{(Bg_0)(t)}dt. \tag{11}$$

Thus, if $v_d = (TT^*)z_d$ then

$$V_d(\omega) = H_d(\omega)Z_d(\omega), \tag{12}$$

where

$$H_d(\omega) = \sum_{k \in \mathcal{Z}} \Pi(\frac{\omega - 2\pi k}{\tau})|G(\frac{\omega - 2\pi k}{\tau})|^2. \tag{13}$$

The $(TT^*)^\dagger$ operation is thus equivalent to discrete-time filtering with a filter of frequency response

$$\begin{cases} \frac{1}{H_d(\omega)} & H_d(\omega) \neq 0 \\ 0 & H_d(\omega) = 0 \end{cases} \tag{14}$$

Combining the frequency domain expressions for T^* and $(TT^*)^\dagger$, we find that the minimum norm least squares (MNLS) solution $\hat{x} = T^*(TT^*)^\dagger z_d$ can be computed in the frequency domain as

$$\hat{X}(\Omega) = R(\Omega)Z_d(\Omega\tau), \tag{15}$$

where

$$R(\Omega) \triangleq \begin{cases} \frac{\Pi(\Omega)G(\Omega)}{H_d(\Omega\tau)} & \text{where } H_d(\Omega\tau) \neq 0 \\ 0 & \text{where } H_d(\Omega\tau) = 0 \end{cases}$$

It is remarkable that the MNLS algorithm is a linear, time-invariant filter even in the absence of any restrictions/bounds on the sampling rate $(\frac{1}{\tau})$ or pulse width Δ.

Conventional wisdom holds that the resolution δ is limited by both τ and Δ, i.e., that to achieve a resolution of δ, not only must the sample spacing τ be less than δ, but the pulse width Δ must also be smaller than δ. The first condition is considered necessary, because the Nyquist sampling frequency for a passband $[\frac{-\pi}{\delta}, \frac{\pi}{\delta}]$ is $\frac{2\pi}{\delta}$ (which means the minimum value of sample spacing τ is δ). The second condition is deemed necessary because of the classical Rayleigh resolution limitations. Two point sources (Dirac delta functions) spaced δ apart are reproduced in the measured signal y_d as a pair of superimposed copies of the measurement kernel g_0 with a relative translation of δ. If the width Δ of kernel g_0 is less than δ, the two copies do not overlap and the two point sources stand out as resolved distinct peaks in y_d.

The following rather simple analysis of the MNLS reconstruction (15) shows that (at least in this ideal noiseless, infinite-data situation), the Rayleigh limit is irrelevant, and that

even if the two point sources do not appear to be resolved in the measured signal y_d, they may be resolved in the reconstruction $\hat{x}$. The analysis shows that in this ideal situation, resolution is determined solely by the sample spacing (i.e., $\delta = \tau$) and is independent of pulse width Δ and even the shape of the sampling kernel g_0.

If τ is smaller than the Nyquist sampling interval for $\mathcal{B}_\delta = [\frac{-\pi}{\delta}, \frac{\pi}{\delta}]$ (or if $g_0(t)$ is bandlimited to $[\frac{-\pi}{\tau}, \frac{\pi}{\tau}]$), then there will be no aliasing in $H_d(\omega)$ in (13). In this case,

$$\begin{aligned} H_d(\omega) &= \Pi(\frac{\omega}{\tau})|G(\frac{\omega}{\tau})|^2 \\ Y_d(\omega) &= X(\frac{\omega}{\tau})\overline{G(\frac{\omega}{\tau})}. \end{aligned} \tag{16}$$

Therefore,

$$R(\Omega) = \begin{cases} \frac{\Pi(\Omega)G(\Omega)}{\Pi(\Omega)|G(\Omega)|^2} = \frac{1}{G(\Omega)} & \text{when } \Pi(\Omega)G(\Omega) \neq 0 \\ 0 & \text{when } \Pi(\Omega)G(\Omega) = 0 \end{cases} \tag{17}$$

and, assuming noise-free observations,

$$\hat{X}(\Omega) = \begin{cases} X(\Omega) & \text{when } \Pi(\Omega)G(\Omega) \neq 0 \\ 0 & \text{when } \Pi(\Omega)G(\Omega) = 0 \end{cases}. \tag{18}$$

From this analysis it is clear that, under noise-free conditions and infinitely many samples, the reconstructed spectrum $\hat{X}(\Omega)$ differs from the true spectrum, $X(\Omega)$ only at the frequencies at which $G(\Omega) = 0$. If $g(t)$ is of finite duration, ($\Delta < \infty$), the *Fourier Uncertainty Principle* states that $G(\Omega)$ cannot be bandlimited i.e. the set of frequencies where $G(\Omega) = 0$, has zero measure. Thus $\hat{X}(\Omega) = X(\Omega)$ *almost everywhere* in this case, which means that the minimum norm reconstruction algorithm has an ideal resolution equal to τ and not pulse width Δ. This result is independent of the shape of the sampling pulse, as long as its support Δ is finite.

From the above analysis, we now see that it is possible to improve resolution in digital mammography and other applications in which the width Δ of the sampling pulse g_0 is greater than the desired resolution, δ, by the use of multiple exposures based on staggering the sampling grid by τ, $\tau < \delta$, with every new exposure. This strategy is illustrated in Figure 1 for a 1D problem with a square sampling pulse. For simplicity of analysis, we assume that the sample-spacing within an exposure is $m\tau$, where m is the number of exposures. Thus, after the m exposures are interleaved, we obtain uniform sampling with

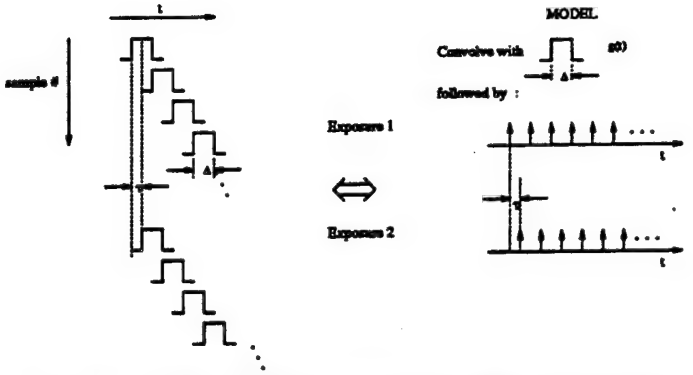

Figure 1: The multi-exposure sampling strategy.

spacing τ which can be a small fraction of Δ. In a 2D application like digital mammography, this strategy requires multiple exposures with 2D translations of the collimators (relative to the object) between exposures. For instance, to improve resolution from 50 microns to 25 microns in each dimension in this 2D problem, we will need 4 staggered exposures. A similar sampling strategy was suggested for tomography and deconvolution applications in [14, 15].

3.1 Effect of noise on resolution

In practice measurements are usually corrupted by noise and, generally, only a finite number of measurements are available, which causes the resolution limit to be affected by the shape and width of the sampling pulse and by the signal-to-noise ratio (SNR). The effects of observation noise on the reconstruction will be considered next while we still assume that infinitely many measurements are available.

If $N_d(\omega)$ is the DTFT of n_d, the noise vector, then in the adequately sampled case (i.e., $\tau < \delta$) the MNLS solution in the frequency domain is given by

$$\hat{X}_{MNLS}(\Omega) = \begin{cases} X(\Omega) + \frac{N_d(\Omega\tau)}{\Pi(\Omega)|G(\Omega)|^2} & \text{where } \Pi(\Omega)G(\Omega) \neq 0 \\ 0 & \text{where } \Pi(\Omega)G(\Omega) = 0 \end{cases} . \tag{19}$$

When the magnitude of $G(\Omega)$ is small, the noise component $(\frac{N_D(\Omega\tau)}{\Pi(\Omega)|G(\Omega)|^2})$ becomes relatively large, which leads to a totally unacceptable and unstable solution. Therefore, regularization is required for an approximate but stable solution. A simple regularization scheme is to zero the solution whenever $|G(\Omega)|$ falls below a certain value. The regularized MNLS solution in this case is

$$\hat{X}_r(\Omega) = \begin{cases} X(\Omega) + \frac{N_d(\Omega\tau)}{\Pi(\Omega)|G(\Omega)|^2} & \text{where } |\Pi(\Omega)G(\Omega)| > \mu \\ 0 & \text{where } |\Pi(\Omega)G(\Omega)| \leq \mu \end{cases} . \tag{20}$$

Depending on the shape of the sampling pulse g_0 (and its width Δ) and on the noise levels, the frequency bands in P_δ where $|G(\Omega)| \leq \mu$ may be large. In these bands, there is a total loss of information about the underlying signal.

Another method of regularization is to add a small positive constant to the denominator of the MNLS solution (15). This approach is popularly known as the Tikhonov regularization method. The MNLS solution with Tikhonov regularization is given by

$$\hat{x}_t = T^*(TT^* + \mu B)^{-1} y_d. \tag{21}$$

In the frequency domain the solution is

$$\hat{X}_t(\Omega) = \frac{\Pi(\Omega)|G(\Omega)|^2 X(\Omega)}{\Pi(\Omega)|G(\Omega)|^2 + \mu} + \frac{N_d(\Omega\tau)}{\Pi(\Omega)|G(\Omega)|^2 + \mu} \quad \mu > 0. \tag{22}$$

The following example illustrates the two types of regularization schemes and their effects on the resolution limit.

Example 3.1 Let $x(t)$ be bandlimited to $[-16\pi, 16\pi]$ with a spectrum as shown in Figure 2. Let the sampling function, $g_0(t)$, be a square-pulse of width $\Delta = \frac{1}{4}$ and let $\tau = \frac{\Delta}{4} = \frac{1}{16}$. Figure 2 shows a plot of $\Pi(\Omega)|G(\Omega)|$. With N_d equal to a constant $\rho = 10^{-4}$ and a regularization parameter $\mu = 25\rho$, the two regularized solutions X_t and X_r are illustrated in Figure 2. ■

In the absence of multiple exposures (with $\tau = \Delta$), the spectrum of $X(\Omega)$ could have been recovered only up to frequencies in $[\frac{-\pi}{\Delta}, \frac{\pi}{\Delta}]$. Because of multiple interleaved exposures ($\tau = \Delta/4$), we are able to extract information at the higher frequencies as well. From Figure 2 it is evident that X_r is zero over certain frequency bands. It is also clear that when the regularization parameter, μ, is decreased, the size of these missing frequency bands decreases; however, the contribution of noise to the solution is increased. Thus the parameter μ presents a trade-off between these two effects and must be chosen as a compromise between the two. The zeroing of X_r over these bands (however narrow) may be unacceptable in many applications, since it causes oscillatory behavior (often called *ringing*) in the time domain. With the Tikhonov regularization, it is observed that the signal component of the MNLS solution is approximate in the entire frequency region. However, there are no missing bands and the time-domain solution is smoother. Here as well, choice of μ is critical to the reconstruction and is usually made based on the SNR.

Since in the noise-corrupted case, the signal cannot (in general) be perfectly reconstructed, a new measure of resolution is necessary that allows for imperfect reconstruction. We develop a measure of resolution based on the maximum tolerable worst-case error.

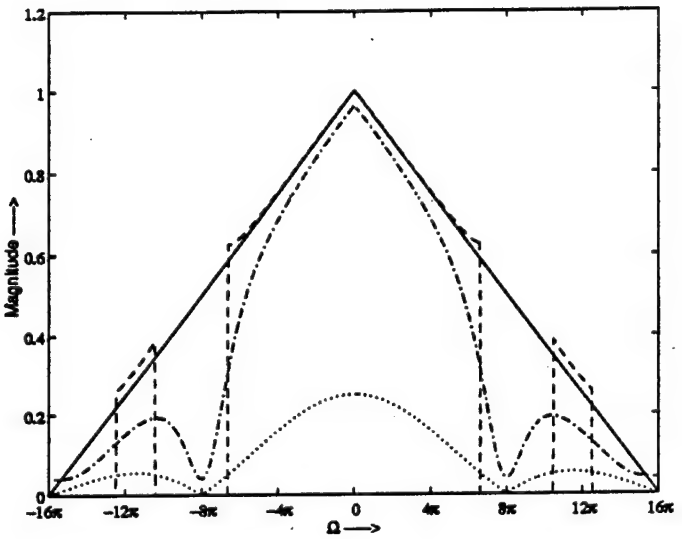

Figure 2: Effects of the spectral truncation and Tikhonov regularization in the frequency domain. —— true spectrum; - - - with spectral truncation; – · —· with Tikhonov scheme; · · · sampling kernel spectrum.

It is obvious that the magnitude of the reconstruction error (even after normalization by signal norm) depends on the magnitude of the measurement noise and on the particular underlying signal. We therefore assume that the SNR is greater than a given positive constant $\frac{1}{\eta^2}$. In other words, we assume that in (4), $\|n_d\|^2 \leq \eta^2 \|Tx\|^2$. Therefore, we define resolution as follows.

Definition 3.2 A certain reconstruction algorithm has *ϵ'-resolution* of δ or better if the worst-case normalized reconstruction error (over all $x \in \mathcal{B}_\delta$ and all n_d such that $\|n_d\| \leq \eta\|Tx\|$) is no larger than ϵ',

$$\frac{\|x - \hat{x}\|^2}{\|x\|^2} \leq \epsilon' \quad \forall x \in \mathcal{B}_\delta;\ \forall n_d : \|n_d\|^2 \leq \eta^2 \|Tx\|^2.$$

■

Note that ϵ'-resolution is defined for a recovery algorithm and not for the recovery problem.

In order to lower-bound the ϵ'-resolution limit for a particular recovery algorithm, we require tight upper bounds for the worst-case normalized reconstruction error. As we shall see, in many situations the upper bound might trivially be 1, unless the feasible set of signals is restricted. For example, let $\mathcal{S} = \{\Omega : |G(\Omega)| \leq \mu\}$. Consider a signal $x \in \mathcal{B}_\delta$ such

that

$$X(\Omega) = \begin{cases} 1 & \Omega \in \mathcal{S} \cap P_\delta \\ 0 & else \end{cases}.$$

For this signal it is clear that $\hat{X}_r(\Omega) = 0 \; \forall \Omega$. Thus, if x is not identically zero, the worst-case normalized error in this case is 1. A less trivial bound on the worst-case error might be found if δ is increased or if we restrict the set of feasible signals by imposing constraints based on known signal properties, such as energy bounds, positivity, bounds on the derivatives, or spectral bounds. We will attempt to obtain this bound in the next section for the practical situation in which only finitely many measurements are available.

4 Resolution in the Practical Situation

In this section we analyze resolution limits for signal recovery problems with *finitely* many *noisy* observations. Let p be the number of measurements available. The measurement process as before is represented by the linear operator $T : L_2(R) \rightarrow C^p$ as

$$(Tx)_i = \langle x, g_i \rangle, \quad i = 1, 2, \ldots, p.$$

The g_i could be uniformly translated versions of a single measurement signal g_0, as in (7), but it is not necessary for this analysis.

The reconstruction problem is formulated as follows

given T, δ, and measurement vector $y_d \in C^p$, find $x \in \mathcal{B}_\delta$ such that $Tx = y_d$.

The set of all signals in $\mathcal{B}_\delta$ satisfying $Tx = y_d$ is a linear variety, $\mathcal{V}$, with finite codimension p. Thus, there are an infinite number of feasible solutions if data-matching is the only constraint. The min-max optimal solution, which is also the minimum norm solution, is given by

$$\begin{aligned} \hat{x}_{MN} &= arg \min_{x \in \mathcal{V}} \|x\| \\ &= T^*(TT^*)^{-1} y_d. \end{aligned}$$

The operator TT^* is now simply a $p \times p$ matrix whose ij^{th} entry is $\langle g_j, g_i \rangle$.

Since the true signal can be any member of $\mathcal{V}$, the supremum of the normalized reconstruction error, $\frac{\|x - \hat{x}_{MN}\|}{\|x\|}$, is 1. Thus our earlier definition of ϵ'-resolution becomes meaningless, since for every y_d and passband $P_\delta = [\frac{-\pi}{\delta}, \frac{\pi}{\delta}]$, we can find a signal $x \in \mathcal{B}_\delta$ for which

the normalized reconstruction error is greater than the tolerable error. Hence, we have to restrict the set of admissible signals appropriately to bound the worst-case error.

However, a finite number of measurements is often justified, because most signals encountered in physical systems are *essentially timelimited.* Accordingly, we restrict our attention to these signals.

Let Γ be a compact set (usually a union of possibly discontiguous closed intervals) in R. Let $W : L_2(R) \rightarrow L_2(R)$ denote the windowing operator to Γ,

$$Wx(t) = \begin{cases} x(t) & t \in \Gamma \\ 0 & \text{else} \end{cases} . \tag{23}$$

Since $\langle Wx, y \rangle = \langle x, Wy \rangle \quad \forall x, y \in L_2(R)$, W is a self-adjoint operator. A signal is said to be ϵ-essentially time-limited to Γ if $\|Wx\|^2 \geq (1-\epsilon)\|x\|^2$. Let $G_{\epsilon,\delta}(\Gamma)$ denote the set of signals which are bandlimited to $[\frac{-\pi}{\delta}, \frac{\pi}{\delta}]$ and ϵ-essentially timelimited to Γ, i.e.,

$$G_{\epsilon,\delta}(\Gamma) \triangleq \{x \in \mathcal{B}_\delta : \|Wx\|^2 \geq (1-\epsilon)\|x\|^2\}. \tag{24}$$

The set $G_{\epsilon,\delta}(\Gamma)$ represents most signals encountered in physical imaging and information systems. Hence, we state the following definition of resolution.

Definition 4.1 A reconstruction algorithm on concentration window Γ and concentration factor $1-\epsilon$ with $SNR \geq \frac{1}{\eta^2}$ will be said to have ϵ'-resolution of δ or better if $\forall x \in G_{\epsilon,\delta}(\Gamma)$ and $\forall n_d \; s.t. \; \|n_d\| \leq \eta\|Tx\|$,

$$\frac{\|x - \hat{x}\|^2}{\|x\|^2} \leq \epsilon'.$$

■

The set $G_{\epsilon,\delta}(\Gamma)$ has several interesting properties which can be exploited to determine resolution limits. Many of these properties are characterized by an orthonormal family of functions called the *Prolate Spheroidal Wave Functions* (PSWFs), $\{\phi_i\}_{i=1}^{\infty}$, and by the associated eigenvalues, $\{\lambda_i\}_{i=1}^{\infty}$ [16], [17]. The PSWFs corresponding to Γ and P_δ are solutions to the following integral equation,

$$\lambda_i \phi_i(t) = \int_\Gamma \frac{sin\frac{2\pi}{\delta}(t-s)}{\pi(t-s)} \phi_i(s) ds. \tag{25}$$

Properties of the PSWF and the associated eigenvalues have been widely studied. The following three properties of the PSWF are essential to the treatment of resolution limits with finite data:

1. ϕ_i's are bi-orthogonal functions, i.e., for $i \neq j$

$$\begin{aligned} \langle \phi_i, \phi_j \rangle &= 0 \\ \langle W\phi_i, W\phi_j \rangle &= 0 \end{aligned}$$

2. $\lambda_1 > \lambda_2 > \lambda_3 \cdots > 0$,

3. $\{\phi_i\}_{i=1}^{\infty}$ form an orthonormal basis for $\mathcal{B}_\delta$.

With $G_{\epsilon,\delta}(\Gamma)$ as the feasible set, the recovery problem becomes

given T, δ and the measurements $y_d \in C^p$, find $x \in G_{\epsilon,\delta}(\Gamma)$ such that $Tx = y_d$.

Since the resolution limit of a recovery algorithm is based on the worst-case relative error, our objective is to find an algorithm that will minimize the worst-case relative error.

4.1 Lower Dimensional Approximation

Consider any signal $x \in G_{\epsilon,\delta}(\Gamma) \subset \mathcal{B}_\delta$. Since the $\{\phi_i\}_{i=1}^{\infty}$ form an orthonormal basis for $\mathcal{B}_\delta$ from property (3), we can express x as

$$x = \sum_{i=1}^{\infty} \alpha_i \phi_i.$$

To recover $x \in G_{\epsilon,\delta}(\Gamma)$, in general, we have to determine an infinite number of α_i, from a finite number (p) of observations. However, every $x \in G_{\epsilon,\delta}(\Gamma)$ satisfies $\frac{\|Wx\|^2}{\|x\|^2} \geq 1 - \epsilon$, and hence we have the following condition on the coefficients α_i,

$$\sum_{i=1}^{\infty} \alpha_i^2 \lambda_i \geq 1 - \epsilon.$$

This condition suggests that we may be able to restrict our reconstructions to a finite-dimensional subspace of $\mathcal{B}_\delta$ (of dimension less than p) and still obtain low error reconstructions. The next theorem, a well-known result, shows that $G_{\epsilon,\delta}(\Gamma)$ is *essentially finite dimensional* and that the PSWF optimally approximate $G_{\epsilon,\delta}(\Gamma)$ [16], [17].

Theorem 4.1 (Landau-Pollak-Slepian) *For any positive integer N, amongst all N-dimensional spaces S_N, the space spanned by the first N PSWF, $S_N^\phi \triangleq span\{\phi_1, \phi_2, \ldots, \phi_N\}$, is optimal for $G_{\epsilon,\delta}(\Gamma)$ in that it minimizes*

$$\max_{x \in G_{\epsilon,\delta}\{\Gamma\}} \min_{\hat{x} \in S_N} \frac{\|x - \hat{x}\|}{\|x\|}. \tag{26}$$

Moreover, the worst-case relative error can be expressed in terms of the eigenvalues associated with the PSWF as

$$E(S_N^\phi) = \begin{cases} 1 & \lambda_{N+1} \geq 1-\epsilon > 0 \\ \frac{\lambda_1-(1-\epsilon)}{\lambda_1-\lambda_{N+1}} & \lambda_{N+1} < 1-\epsilon \leq \lambda_1 \end{cases} . \tag{27}$$

$E(S_N^\phi)$ is also called the N-width of the set $G_{\epsilon,\delta}(\Gamma)$ or the intrinsic error at dimension N. ■

Thus, for a fixed dimension, r, the subspace spanned by the $\{\phi_i\}_{i=1}^r$ minimizes the worst-case relative error. Moreover the worst-case relative error $E(S_r^\phi)$ decreases with r. Thus it would seem that, given p observations, the best choice of a lower dimensional subspace to approximate $G_{\epsilon,\delta}(\Gamma)$ would be $S_p^\phi = \text{span}\{\phi_1, \cdots, \phi_p\}$. This choice would lead to p equations in p unknowns. Unfortunately, the p parameters required to describe the reconstruction from S_p^ϕ cannot be determined exactly from the observations y_d for two reasons. First, y_d are noise-corrupted in practice. Second, the observations y_d are linearly related to $x \in G_{\epsilon,\delta}(\Gamma)$ and not to the projection x_p of x onto S_p^ϕ. Thus, an additional error will be incurred in determining the parameters that describe the lower dimensional approximate. We next derive an expression for this error and its worst-case value $\Xi(r)$ for a fixed dimension r. We suggest choosing r to minimize $E(S_r^\phi) + \Xi(r)$.

4.2 Worst-Case Error Analysis for Subspace Selection

Consider the reconstruction based on an r-dimensional approximation of $G_{\epsilon,\delta}(\Gamma)$, where $r \leq p$, and let x_r be the projection of x onto S_r^ϕ. Then,

$$x_r = \sum_{i=1}^{r} \alpha_i \phi_i \tag{28}$$

and the approximation error $e_r \stackrel{\Delta}{=} x - x_r = \sum_{i=r+1}^{\infty} \alpha_i \phi_i$. In this section, we study the effect of measurement noise and approximation error e_r on the estimate of $\{\alpha_i\}_{i=1}^r$ from measurements y_d. The measurements y_d are linearly related to x and corrupted by noise n_d:

$$\begin{aligned} y_d &= Tx + n_d \\ &= Tx_r + Te_r + n_d \\ &= \sum_{i=1}^{r} \alpha_i T\phi_i + (Te_r + n_d) \\ &= A_r \alpha^r + (Te_r + n_d), \end{aligned} \tag{29}$$

where A_r is a $p \times r$ matrix with $A_r(i,j) = \langle \phi_j, g_i \rangle$, $\alpha^r = (\alpha_1, \cdots \alpha_r)^T$. We will assume that the columns of A_r are linearly independent. If they are not, the worst-case error is unbounded. The LS solution of $T\hat{x} = y_d$, $\hat{x} \in S_r^\phi$, is determined from the MNLS solution of $A_r \hat{\alpha}^r = y_d$, which is

$$\begin{aligned} \hat{\alpha}^r &= A_r^\dagger y_d \\ &= \alpha^r + A_r^\dagger (T e_r + n_d), \end{aligned}$$

where $A_r^\dagger = (A_r^H A_r)^{-1} A_r^H$. Thus the reconstruction is given by

$$\hat{x}_r = \sum_{i=1}^{r} \hat{\alpha}_i^r \phi_i \tag{30}$$

and $\zeta_r = x_r - \hat{x}_r = \sum_{i=1}^{r} (\hat{\alpha}_i^r - \alpha_i)\phi_i$ is the additional error incurred in determining the α_i parameters. The error term, ζ_r, has contributions from both Te_r and measurement noise n_d.

Thus the total reconstruction error is

$$\begin{aligned} \|x - \hat{x}_r\|^2 &= \|x - x_r + x_r - \hat{x}_r\|^2 \\ &= \|e_r + \zeta_r\|^2 \\ &= \|e_r\|^2 + \|\zeta_r\|^2 \quad \text{since } e_r \perp S_r^\phi \text{ and obviously } \zeta_r \in S_r^\phi. \end{aligned}$$

A pictorial representation of these error terms is given in Figure 3. We seek an upper bound

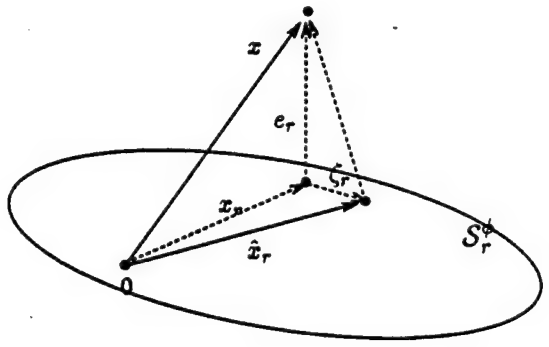

Figure 3: Error terms.

on $\frac{\|x-\hat{x}_r\|^2}{\|x\|^2}$. From Theorem 4.1, it is clear that $\forall x \in G_{\epsilon,\delta}(\Gamma)$,

$$\frac{\|e_r\|^2}{\|x\|^2} \leq E(S_\phi^r) = \begin{cases} 1 & \lambda_{N+1} \geq 1-\epsilon > 0 \\ \frac{\lambda_1-(1-\epsilon)}{\lambda_1-\lambda_{N+1}} & \lambda_{N+1} < 1-\epsilon \leq \lambda_1 \end{cases}$$

All that remains to be done is to upper-bound $\frac{\|\zeta_r\|^2}{\|x\|^2}$. This error term can be interpreted as a penalty on complexity. The complexity in this case is the dimension of the subspace. Recall that $\zeta_r = \sum_{i=1}^{r}(\hat{\alpha}_i^r - \alpha_i)\phi_i$ and that $\hat{\alpha}^r - \alpha^r = A_r^\dagger(Te_r + n_d)$. Hence,

$$\begin{aligned} \|\zeta_r\|^2 &= \|\hat{\alpha}^r - \alpha^r\|^2 \\ &= \|A_r^\dagger(Te_r + n_d)\|^2 \\ &\leq \|A_r^\dagger Te_r\|^2 + \|A_r^\dagger n_d\|^2 + 2\|A_r^\dagger Te_r\|\,\|A_r^\dagger n_d\|, \end{aligned} \tag{31}$$

with equality achieved when $A_r^\dagger n_d$ is collinear with $A_r^\dagger Te_r$. If a lower bound $(\frac{1}{\eta^2})$ on SNR is known, then

$$\begin{aligned} \|n_d\|^2 &\leq \eta^2\|Tx\|^2 \\ &\leq \eta^2\sigma_{max}(TT^*)\,\|x\|^2, \end{aligned}$$

with equality achieved when x is the singular vector of T that corresponds to its maximum singular value $\sqrt{\sigma_{max}(TT^*)}$. Now all that remains to be done is to obtain a tight upper bound on $\frac{\|A_r^\dagger Te_r\|}{\|x\|}$ over $x \in G_{\epsilon,\delta}(\Gamma)$. A loose upper bound may be obtained by using $\|A_r^\dagger Te_r\| \leq \frac{\sqrt{\sigma_{max}(TT^*)}}{\sigma_{min}(A_r)}\|e_r\|$, but we can achieve a better bound because e_r has less than λ_r of its energy in Γ. Mathematically, our objective is to find

$$\sup_{\substack{\sum_{i=1}^{\infty}\alpha_i^2=1 \\ \sum_{i=1}^{\infty}\alpha_i^2(1-\lambda_i)\leq\epsilon}} \|\sum_{i=r+1}^{\infty}\alpha_i A_r^\dagger T\phi_i\|^2. \tag{32}$$

This is a nonlinear infinite programming problem, and in general we can seek only approximate solutions. We devote the remaining of this section to that task. We first show that under mild conditions, the problem can be approximated by a *finite variable* nonlinear programming problem. We then apply well-known techniques to solve the problem. We start with the following definition.

Definition 4.2 An observation made with a measurement functional, g, is in the concentration window, Γ, if support(g) $\subset \Gamma$

Lemma 4.1 [18] *The eigenvalues $\{\lambda_i\}$ associated with the PSWF corresponding to a pass-band $[\frac{-\pi}{\delta}, \frac{\pi}{\delta}]$ and a compact concentration window Γ are absolutely summable and*

$$\sum_{k=1}^{\infty} \lambda_k = \frac{2}{\delta} \int_{\Gamma} dt. \tag{33}$$

■

Lemma 4.2 *Let $x \in G_{\epsilon,\delta}(\Gamma)$ with $x = \sum_{k=1}^{\infty} \alpha_k \phi_k$ and $\|x\|^2 = \sum_{k=1}^{\infty} \alpha_k^2 = 1$. Let $e_N \triangleq \sum_{k=N+1}^{\infty} \alpha_k \phi_k$*

If all the measurements are taken in the concentration window, Γ, i.e., every g_i has a support inside the concentration region Γ, then there exists a finite number M such that for every positive integer N,

$$\|Te_N\|^2 \leq M(\sum_{k=N+1}^{\infty} \lambda_k),$$

and $\lim_{N\to\infty} \|Te_N\|^2 = 0$. In fact, $\|TT^*\|$ will serve as M. ■

Thus as N becomes large the contribution of Te_N becomes negligible in the error.

Theorem 4.2 *Let $\gamma > 0$ and the rest of the assumptions be as stated in Lemma 4.2. There exists a positive integer N independent of the choice of $x \in G_{\epsilon,\delta}(\Gamma)$ such that*

$$\|A_r^{\dagger} T e_r\| - \| \sum_{i=r+1}^{N} \alpha_i A_r^{\dagger} T \phi_i \| \leq \gamma. \tag{34}$$

Furthermore,

$$\sup_{x \in G_{\epsilon,\delta}(\Gamma)} \frac{\|A_r^{\dagger} T e_r\|}{\|x\|} = \gamma + \sup_{\substack{\sum_{i=1}^{N} \alpha_i^2 = 1 \\ \sum_{i=1}^{N} \alpha_i^2 (1-\lambda_i) = \epsilon}} \| \sum_{i=r+1}^{N} \alpha_i A_r^{\dagger} T \phi_i \|. \tag{35}$$

■

Proofs of Lemma 4.2 and Theorem 4.2 can be found in the appendix.

Theorem 4.2 shows that the solution to the infinite programming problem in (32) can be approximated closely by a sufficiently large finite variable problem. Let N, sufficiently large, be chosen, let $H_N \triangleq [h_1, h_2, \cdots h_N]$ be a $p \times N$ matrix with columns h_i given by

$$h_i = \begin{cases} 0 & 1 \le i \le r \\ A_r^\dagger T\phi_i & r+1 \le i \le N \end{cases}, \tag{36}$$

and let $\Lambda_N = \mathrm{diag}([\lambda_1, \lambda_2, \cdots, \lambda_N])$. Then a bound on $\|A_r^\dagger T e_r\|$ can be obtained by computing

$$m_r = \max_{\substack{\|\Lambda_N^{\frac{1}{2}}\alpha^N\|^2 = 1-\epsilon \\ \|\alpha^N\|=1}} \|H_N \alpha^N\| \tag{37}$$

A popular method for solving this nonlinearly constrained quadratic program is the *sequential quadratic programming* method, [13], [19].

Let $b_r \triangleq (\gamma + m_r)^2$ and define the noise contribution factor $\rho_r^2 \triangleq \frac{\sigma_{max}(TT^*)}{\sigma_{min}^2}$. Then $\|A_r^\dagger T e_r\|^2 \le b_r \|x\|^2$ and from (31),

$$\begin{aligned} \|\zeta_r\|^2 &\le \|A_r^\dagger T e_r\|^2 + \|A_r^\dagger n_d\|^2 + 2\|A_r^\dagger T e_r\| \, \|A_r^\dagger n_d\| \\ &\le \left(b_r + \frac{\sigma_{max}(TT^*)}{\sigma_{min}^2(A_r)}\eta^2 + 2\sqrt{\frac{\sigma_{max}(TT^*)}{\sigma_{min}^2(A_r)}\eta^2 b_r} \right) \|x\|^2 \\ &= (b_r + \rho_r^2\eta^2 + 2\sqrt{b_r\rho_r^2\eta^2})\|x\|^2 \\ &\triangleq \Xi(r)\|x\|^2, \end{aligned} \tag{38}$$

where $\Xi(r) \triangleq b_r + \rho_r^2\eta^2 + 2\sqrt{b_r\rho_r^2\eta^2}$. Hence, we have the following procedure for determining $\Xi(r)$, using the PSWF, ϕ_i, the corresponding eigenvalues λ_i, and an acceptable value of γ

For each candidate dimension r,

- construct the $p \times r$ matrix $A_r = [T\phi_1 T\phi_2 \cdots T\phi_r]$ and compute its smallest singular value, σ_{min}.
- Find the smallest integer N for which

$$\frac{2}{\delta}\int_\Gamma dt - \sum_{k=1}^{N} \lambda_k \le \frac{\sigma_{min}^2\gamma^2}{\|TT^*\|}.$$

- Construct H_N as in (36), and let $\Lambda_N = \mathrm{diag}([\lambda_1, \lambda_2, \cdots, \lambda_N])$. Solve (37) by the sequential quadratic programming method and let $b_r = (\gamma + m_r)^2$.
-

$$\Xi(r) \triangleq b_r + \rho_r^2\eta^2 + 2\sqrt{b_r\rho_r^2\eta^2} = (\sqrt{b_r} + \rho_r\eta)^2. \tag{39}$$

Thus a bound on the worst-case normalized error, $\Theta(r)$, can be obtained by the sum of the intrinsic error and a bound on the worst-case $\|\zeta_r\|^2$, i.e.,

$$\Theta(r) = \min(1, E(S_\phi^r) + \Xi(r)). \tag{40}$$

Thus, to ascertain whether a resolution of δ can be achieved given a set of p measurements, we first compute the bound on the worst-case normalized error bounds for each dimension r ranging from 1 through p using the PSWF corresponding to $P_\delta = [\frac{-\pi}{\delta}, \frac{\pi}{\delta}]$ and we determine the dimension r^* which gives the smallest error. If the worst-case error for this dimension is below the allowable error, we can claim that a resolution of δ can be achieved with the given set of measurements and noise level.

Remarks:

1. As a consequence of the above analysis we have a new algorithm for signal recovery based on dimension reduction guided by the bound on the worst-case reconstruction error.

2. The worst-case error-bound given by (40) does not depend on the data y_d. It depends only on the sampling functions, g_i, the bandwidth, $\frac{2\pi}{\delta}$, the sample spacing, τ, the noise level, η, and the choice of the dimension, r. Thus, the selection of the dimension and the determination of resolution can be made (off-line) before the measurements are taken.

3. Our analysis and definition of resolution are based on worst-case errors in a deterministic framework. Therefore, in general the reconstruction error can be expected to be lower than the predicted value.

4. The analysis holds true for all sampling patterns. Hence g_i, the i^{th} measurement function, does not have to be a shifted version of a single measurement function g_0. The only restriction is that the support of each g_i lies inside the concentration window, Γ.

5. We have assumed essential timelimitedness and strict bandlimitedness in our treatment, which can be easily changed to essential timelimitedness to Γ and essential bandlimitedness to P. The PSWF will still be the optimal sequences, [20] and all the results will still hold true, with minor modifications.

6. The PSWF have been studied in the classical setting of 1D signals with lowpass passband and contiguous concentration intervals. The three relevant properties of the

PSWF and the dimensionality theorem can be generalized to the more general setting of mD signals with P and Γ discontiguous. They follow by expressing the integral equation, (25) as a linear operator equation, as follows [21], [22]

$$\begin{aligned} WBW\psi_i &= \lambda_i\psi_i \\ \lambda_i\phi_i &= BW\psi_i \end{aligned} \tag{41}$$

Recognizing that the ψ_i are the eigenvectors of a positive semidefinite operator with eigenvalues λ_i, the following three properties of the PSWF which are essential to this analysis become obvious:

- the ϕ_i's are biorthogonal functions, i.e., for $i \neq j$

$$\begin{aligned} \langle \phi_i, \phi_j \rangle &= 0 \\ \langle W\phi_i, W\phi_j \rangle &= 0 \end{aligned}$$

- $\lambda_1 > \lambda_2 > \lambda_3 \cdots > 0$.
- $\{\phi_i\}_{i=1}^{\infty}$ forms an orthonormal basis for $\mathcal{B}_P$, the space of finite-energy signals bandlimited to P.

Since the dimensionality theorem uses only these three properties, it can be generalized as well.

4.3 Implementation Details

In practice, all integrals have to be computed using numerical approximation methods. We use simple summation after discretizing functions on a fine grid. With discretization, the PSWF computation of (41) becomes an eigenvalue-eigenvector computation followed by low-pass filtering [23]. Constructing the entries of the matrices A_r, H_N and TT^* requires computation of integrals and is also achieved by discretization and summation.

In the 2D case, if the passband is square, the kernel in the integral equation, (25), describing the PSWF becomes separable. If in addition the concentration region is also square, the double integral in (25) becomes

$$\mu_k\Phi_k(t,s) = \int_{-T/2}^{T/2}\int_{-T/2}^{T/2} \frac{sin\frac{2\pi}{\delta}(t-\tau_1)}{\pi(t-\tau_1)} \frac{sin\frac{2\pi}{\delta}(t-\tau_2)}{\pi(t-\tau_2)} \Phi_k(\tau_1,\tau_2)\, d\tau_1 d\tau_2, \tag{42}$$

where Φ_k is the k^{th} 2D PSWF with associated eigenvalue μ_k. If the ϕ_i are the 1D PSWF corresponding to δ and $\Gamma = [-T/2, T/2]$, then it is clear that for each i, j, $\Phi(t,s) = \phi_i(t)\phi_j(s)$ satisfies (42) with $\mu = \lambda_i\lambda_j$. Thus after discretization, if we represent each 2D PSWF as a long 1D vector of columns stacked one below the other, then the 2D PSWFs can be

computed as Kronecker products of corresponding 1D PSWFs taken two at a time with eigenvalues equal to the product of the corresponding eigenvalues.

We next illustrate these results and the computational details in two examples. The first example is in a 1D setting. The second example is in a 2D setting to illustrate the applicability of the results to multiple dimensions.

Example 4.1 (1D setting) Consider reconstruction of 1D signals that are bandlimited to $[-4\pi, 4\pi]$ and have at least 99.5% of their energy concentrated in $[-2.0, 2.0]$, from 19 measurements taken with shifted unit rectangular pulses of width $\frac{1}{2}$ and interpulse distance (stagger) $\frac{1}{4}$. Thus δ, Γ, and ϵ are $\frac{1}{4}$, $[-2.0, 2.0]$ and 0.005 respectively in the definition of $G_{\epsilon,\delta}(\Gamma)$, while p and τ are 19 and $\frac{1}{4}$. The sampling functions are

$$g_k(t) = g_0(t - \frac{k}{4}) \quad k = 1, 2, \ldots 19,$$

where

$$g_0(t) = \begin{cases} 1 & 0 \leq t \leq 0.5 \\ 0 & \text{else} \end{cases}.$$

Note that the width of the sampling pulses is $\frac{1}{2} = 2\delta$. Thus the Rayleigh resolution limit is 2δ. Let the error tolerance be 10%. We will see that, at an SNR of 40dB, a resolution limit of $\tau = \frac{1}{4}$ (better than the Rayleigh limit) can be achieved by the proposed algorithm.

The nonlinear programming problem of (37) is solved by using the sequential quadratic programming method. The intrinsic error $E(S_r^\phi)$, the parameter estimation error without noise b_r, the noise contribution factor ρ_r, are computed for each dimension, r, for which $E(S_r^\phi) < 1$. The values are tabulated in Table 4.1 along with $\Theta(r) = E(S_r^\phi) + (\sqrt{b_r} + \rho_r \eta)^2$ for SNR of 32 dB and 40 dB. From the table we observe that, with a 40dB SNR, the optimal dimension for this signal recovery problem is 15, and the worst-case normalized error is bounded above by 0.0531. In fact, using (39, 40), we can show that with a 10% error allowance, a resolution of at least $\tau = 0.25$ can be achieved by the above algorithm whenever the SNR is greater than 32dB. As remarked earlier, all these computations can be done off-line, since they do not depend on the actual observed data.

We now test the reconstruction algorithm using the precomputed optimal dimension of 15 on a specific signal,

$$x(t) = \left(\frac{sin(0.4\pi t)}{0.4\pi t}\right)^2 + 0.2\frac{sin(0.1\pi t)}{0.1\pi t} cos(3.5\pi t).$$

Table 1: Intrinsic error, noise factor and total error versus dimension.

r	$E(S_r^{\varphi})$	b_r	noise-factor ρ_r	$\Theta(r)$ SNR=40dB	$\Theta(r)$ SNR=32dB
13	0.2203	0.1905	4.3953	0.4511	0.5188
14	0.0379	0.0430	5.4552	0.1065	0.1561
15	0.0100	0.0189	7.0128	0.0531	0.1078
16	0.0046	0.0338	9.4899	0.0823	0.1819
17	0.0034	0.0788	13.2808	0.1744	0.3788
18	0.0032	0.1103	17.6118	0.2615	0.5998
19	0.0031	0.1124	27.8416	0.3797	1.0000

A plot of the signal is shown in Figure 4 (a). The highest frequency in $x(t)$ is 3.6 radians. Note that $x(t)$ is a low frequency signal with a low energy, high-frequency ripple. The frequencies are selected in order that the low-frequency component falls below the Rayleigh limit and, hence, is captured by the observations, whereas the high-frequency ripple is much above the Rayleigh limit and thus is not seen in the observations (Figure 4 (b)). A high resolution reconstruction should resolve the high frequency ripple, also. Since $x(t)$ has 99.69 % of its energy inside the concentration interval $[-2.0, 2.0]$, i.e., $\epsilon = 0.0031$, it belongs to the set $G_{\epsilon,\delta}(\Gamma)$ considered in this example. We take 19 observations in the concentration window with shifted versions of the sampling function described by (4.1). The observations are shown in Figure 4(b). Note that the high-frequency ripple is completely lost in the observations.

The reconstruction, $\hat{x}$, is computed using the algorithm with precomputed dimension of 15. It is also depicted in Figure 4 (a). The normalized error for this reconstruction, $(\frac{\|x-\hat{x}\|}{\|x\|})^2$, is computed to be 0.0068, which is much less than the worst-case error bound of 0.0531. ■

We now consider an example in two dimensions.

Example 4.2 (2D setting) Consider the reconstruction problem for 2D signals that are bandlimited to a square passband $P_\delta = [-2\pi, 2\pi] \times [-2\pi, 2\pi]$ and have at least 99% of their energy inside the square region $[-2.5, 2.5] \times [-2.5, 2.5]$ from 121 measurements. The measurements were taken using pulse sampling functions with a square region of support of width 1 and an intersampling distance of $\frac{1}{2}$ in each direction. Since the sample spacing ($\frac{1}{2}$) is smaller than the sampling kernels' width (=1), this sampling strategy requires interleaving

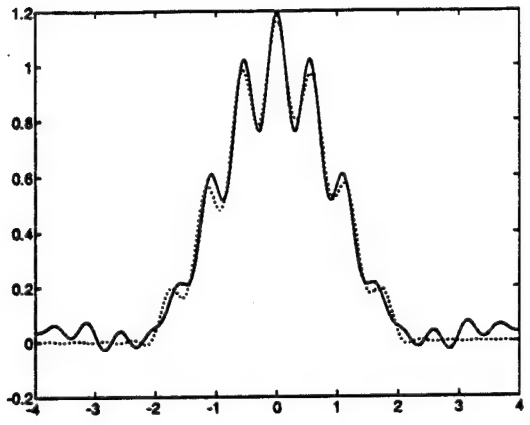

(a)

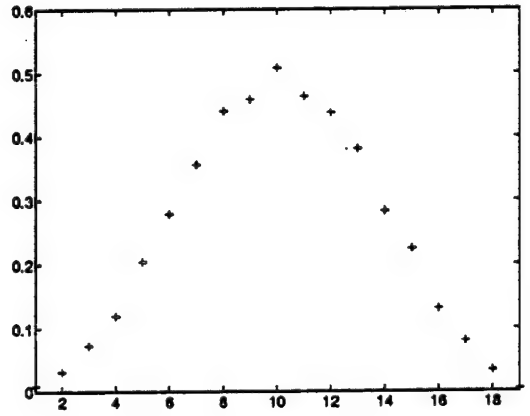

(b)

Figure 4: Reconstruction of the test signal using the optimal dimension determined by the worst-case error analysis. The SNR is 40db. (a) —— signal, $x(t)$; $\cdots\cdots$ reconstruction, $\hat{x}(t)$ (b) + Observations.

of multiple (four) staggered exposures as in Figure 1. The sampling functions are

$$g_{l,k}(t,s) = g_0(t - \frac{l}{2}, s - \frac{k}{2}) \quad l,k = 1,2,\ldots 11,$$

where

$$g_0(t,s) = \begin{cases} 1 & 0 \le t \le 1, 0 \le s \le 1 \\ 0 & \text{else} \end{cases}.$$

With this sampling kernel, the Rayleigh limit will be 1 in each dimension. Let measurements be taken from the concentration window with $\eta = \frac{1}{100}$. This value of η corresponds to an SNR of 40 dB.

The nonlinear programming problem of (37) is solved using the sequential quadratic programming method, and $E(S_r^{\phi})$, $\Xi(r)$, and $\Theta(r)$ are computed for each dimension r for which $E(S_r^{\phi})$ is less than 1. These values are plotted in Figure 5. From the figure we

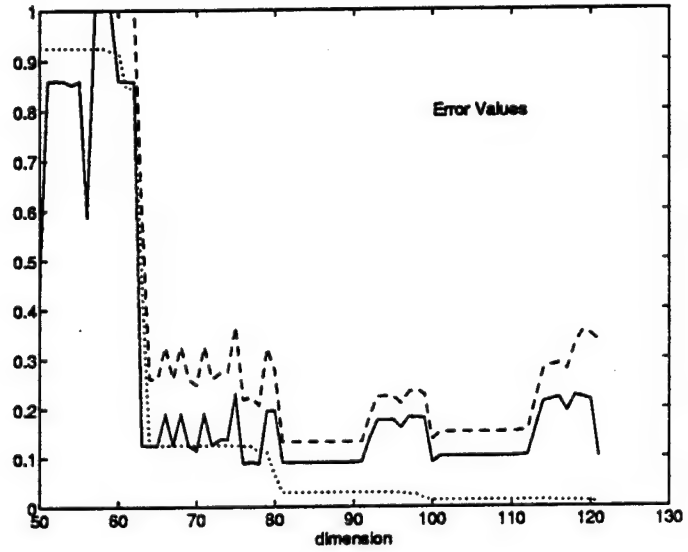

Figure 5: Intrinsic error, $E(r)$ $\cdots$; parameter approximation error, $\Xi(r)$ ——; total error, $\Theta(r)$ - - - - -.

observe that the optimal dimension for this signal recovery problem with a 40dB SNR is any dimension between 81 and 89. The worst-case normalized error in the noisy situation (40dB SNR) is 0.1326. Thus, if an error of 13.5% is tolerable, then a resolution of $\tau = 0.25$ can be achieved by the above algorithm.

Now consider a specific signal in $G_{\epsilon,\delta}(\Gamma)$: $x(t,s) = h(t)h(s)$ with

$$h(t) = 0.25\left(\frac{sin(0.2\pi t)}{0.2\pi t}\right)^2 + 0.05\frac{sin(0.2\pi t)}{0.2\pi t}cos(1.75\pi t).$$

A meshplot of the $x(t,s)$ is shown in Figure 7. As in the 1D case, the signal is comprised of a low-frequency component with a high-frequency ripple. The observations are four exposures with stagger, and they are as shown in Figure 6. The interleaved observations are also shown in Figure 6. The reconstruction using dimension 81 is shown in Figure 7. The relative error is computed to be 0.0179, which is much below the computed upper bound. ■

5 Conclusions

A resolution analysis for signal recovery from finitely many discrete, noise-corrupted, linear measurements is presented. A new measure for resolution is introduced, which is more appropriate than the Rayleigh resolution limit for current signal recovery algorithms. This resolution measure is based on a prescribed tolerance of relative error in the reconstruction, and unlike previous definitions is able to bring out the extent to which time or spatial domain features can be recovered by an algorithm. The computation of resolution limits reduces to the computation of the worst-case relative error in the recovered signal. By suitably constraining the class of feasible signals, the worst-case error is expressed as the solution of a finite-variable nonlinear program. The analysis and examples show that details finer than the Rayleigh resolution limit can be recovered by simple linear processing even in practical situations with finite, noise-corrupted data. In the process, we derive an algorithm for high resolution reconstruction (from linear observations) and show how one can precompute worst-case error bounds and the resolution limit for the algorithm.

Appendix

Proof of Lemma 4.1: Since all the measurements are taken inside the concentration region, $Tx = TWx$, $\forall x \in G_{\epsilon,\delta}(\Gamma)$. Therefore,

$$\begin{aligned}
\|Te_N\|^2 &= \| \sum_{k=N+1}^{\infty} \alpha_k T\phi_k \|^2 \\
&= \|T \sum_{k=N+1}^{\infty} \alpha_k W\phi_k \|^2 \\
&\leq \|TT^*\| \sum_{k=N+1}^{\infty} \alpha_k^2 \|W\phi_k\|^2 \\
&\leq M \sum_{k=N+1}^{\infty} \lambda_k \quad \text{where } M = \|TT^*\|
\end{aligned}$$

Lemma 4.1 and property (2) of the PSWF together show that $\lim_{N\to\infty} \|Te_N\|^2 = 0$. ■

Proof of Theorem 4.2: Let $\sigma_{min} \geq 0$ be the smallest singular value of A_r. By Lemma 4.1

it is possible to choose N such that $\sum_{k=N+1}^{\infty} \lambda_k < \frac{\sigma_{min}^2 \gamma^2}{\|TT^*\|}$. Then,

$$\begin{aligned}
\|A_r^\dagger T e_r\| &= \| \sum_{i=r+1}^{N} \alpha_i A_r^\dagger T \phi_i + \sum_{i=N+1}^{\infty} \alpha_i A_r^\dagger T \phi_i \| \\
&\leq \| \sum_{i=r+1}^{N} \alpha_i A_r^\dagger T \phi_i \| + \|A_r^\dagger T e_N\| \\
p &\leq \| \sum_{i=r+1}^{N} \alpha_i A_r^\dagger T \phi_i \| + \|A_r^\dagger\| \|T e_N\| \\
&\leq \| \sum_{i=r+1}^{N} \alpha_i A_r^\dagger T \phi_i \| + \frac{1}{\sigma_{min}} \sqrt{M \sum_{i=N+1}^{\infty} \lambda_i} \quad \text{(by Lemma 4.2)} \\
&\leq \| \sum_{i=r+1}^{N} \alpha_i A_r^\dagger T \phi_i \| + \gamma \qquad (43)
\end{aligned}$$

Next,

$$\begin{aligned}
\sup_{x \in G_{\epsilon,\delta}(\Gamma)} \frac{\|A_r^\dagger T e_r\|}{\|x\|} &= \sup_{\substack{\sum_{i=1}^{\infty} \alpha_i^2 = 1 \\ \sum_{i=1}^{\infty} \alpha_i^2 (1-\lambda_i) \leq \epsilon}} \| \sum_{i=r+1}^{\infty} \alpha_i A_r^\dagger T \phi_i \| \\
&\leq \sup_{\substack{\sum_{i=1}^{\infty} \alpha_i^2 = 1 \\ \sum_{i=1}^{\infty} \alpha_i^2 (1-\lambda_i) \leq \epsilon}} \| \sum_{i=r+1}^{N} \alpha_i A_r^\dagger T \phi_i \| + \gamma \quad \text{(from 43)} \\
&\leq \sup_{\substack{\sum_{i=1}^{N} \alpha_i^2 \leq 1 \\ \sum_{i=1}^{N} \alpha_i^2 (1-\lambda_i) \leq \epsilon}} \| \sum_{i=r+1}^{N} \alpha_i A_r^\dagger T \phi_i \| + \gamma \qquad (44) \\
&= \sup_{\substack{\sum_{i=1}^{N} \alpha_i^2 = 1 \\ \sum_{i=1}^{N} \alpha_i^2 (1-\lambda_i) = \epsilon}} \| \sum_{i=r+1}^{N} \alpha_i A_r^\dagger T \phi_i \| + \gamma \qquad (45)
\end{aligned}$$

Inequality (44) follows from the fact that the set $\mathcal{S}_1 = \{\alpha : \sum_{i=1}^{\infty} \alpha_i^2 = 1; \sum_{i=1}^{\infty} \alpha_i^2 (1-\lambda_i) \leq \epsilon\}$ is contained in the set $\mathcal{S}_2 = \{\alpha : \sum_{i=1}^{N} \alpha_i^2 = 1; \sum_{i=1}^{N} \alpha_i^2 (1-\lambda_i) \leq \epsilon\}$ and hence the supremum over $\mathcal{S}_2$ is greater than the supremum over $\mathcal{S}_1$. Equality (45) follows because $\| \sum_{i=r+1}^{N} \alpha_i A_r^\dagger T \phi_i \|$ is a convex function in α, and a convex function maximized over a convex set achieves its maximum at the boundary of the convex set. ■

References

[1] J. Von Neumann, *Functional Operators (Vol. II).* Ann. Math. Studies, New Jersey: Princeton University Press, 1950.

[2] R. W. Gerchberg, "Super-resolution through error energy reduction," *Opt. Acta*, vol. 21, no. 9, pp. 709–720, 1974.

[3] A. Papoulis, "A new algorithm in spectral analysis and band-limited extrapolation," *IEEE Trans. Circuits Syst.*, vol. CAS-22, pp. 735–742, September 1975.

[4] J. L. C. Sanz and T. S. Huang, "Discrete and continuous band-limited signal extrapolation," *IEEE Trans. Acoust., Speech & Signal Process.*, vol. ASSP-31, pp. 1276–1285, October 1983.

[5] D. P. Kolba and T. W. Parks, "Optimal estimation of band-limited signals including time domain considerations," *IEEE Trans. Acoust., Speech & Signal Process.*, vol. ASSP-31, pp. 113–122, February 1983.

[6] L. C. Potter and K. S. Arun, "Energy concentration in band-limited extrapolation," *IEEE Trans. Acoust., Speech & Signal Process.*, vol. ASSP-37, pp. 1027–10, July 1989.

[7] D. C. Youla and H. Webb, "Image restoration by the method of convex projections: Part 1 - theory," *IEEE Trans. Med. Imaging*, vol. MI-1, pp. 81–94, October 1982.

[8] L. C. Potter and K. S. Arun, "A dual approach to linear inverse problems with convex constraints," *SIAM J. Control and Optimization*, vol. 31, pp. 1080–1092, July 1993.

[9] S. Dharanipragada and K. S. Arun, "A quadratically convergent algorithm for convex constrained signal reconstruction," *IEEE Trans Sig. Proc.* Under review.

[10] P. A. Jansson, *Deconvolution: With Applications in Spectroscopy.* Orlando, Florida: Academic Press, 1984.

[11] L. S. Joyce and W. L. Root, "Precision bounds in superresolution processing," *J. Opt. Soc. Am. A*, vol. 1, pp. 149–168, February 1984.

[12] W. L. Root, "Ill-posedness and precision in object-field reconstruction problems," *J. Opt. Soc. Am. A*, vol. 4, pp. 171–179, January 1987.

[13] D. G. Luenberger, *Optimization by Vector Space Methods.* New York: Wiley, 1969.

[14] G. Jacquemod, C. Odet, and R. Goutte, "Superresolution technique applied to CCD sensors," in *SIGNAL PROCESSING IV: Theories and Applications* (J. Lacoume, A. Chehikian, N. Martin, and J. Malbos, eds.), pp. 847–850, Elsevier Science Publishers B. V. (North Holland), 1988.

[15] G. Jacquemod, C. Odet, F. Peyrin, and R. Goutte, "Improve resolution of industrial X-ray computed tomographic 3D images," in *Proc. 12th World Conference on Nondestructive Testing* (J. Boogaard and G. M. van Dijk, eds.), pp. 74–79, Elsevier Science Publishers B. V., Amsterdam, 1989.

[16] D. Slepian and H. O. Pollak, "Prolate spheroidal wave functions, Fourier analysis and uncertainty - I," *Bell Syst. Tech. J.*, vol. 40, pp. 43–64, Jan. 1961.

[17] H. J. Landau and H. O. Pollak, "Prolate spheroidal wave functions, Fourier analysis and uncertainty - II," *Bell Syst. Tech. J.*, vol. 40, pp. 65–84, Jan. 1961.

[18] A. W. Naylor and G. R. Sell, *Linear operator theory in engineering and science.* New York: Springer-Verlag, 1982.

[19] P. E. Gill, W. Murray, and M. H. Wright, *Practical Optimization.* New York: Academic Press, 1981.

[20] A. A. Melkman and C. A. Micchelli, "Optimal estimation of linear operators in Hilbert spaces from inaccurate data," *SIAM J. Numer. Anal.*, vol. 16, pp. 87–105, February 1979.

[21] S. Dharanipragada and K. S. Arun, "Signal reconstruction using time-bandwidth dimension,," *IEEE Trans. Sig. Proc.* Under review.

[22] S. Dharanipragada, "Time-bandwidth dimension and its application to signal reconstruction," Master's thesis, University of Illinois, Urbana, IL, 1991.

[23] C. T. H. Baker, *The Numerical treatment of integral equations.* Oxford: Clarendon Press, 1977.

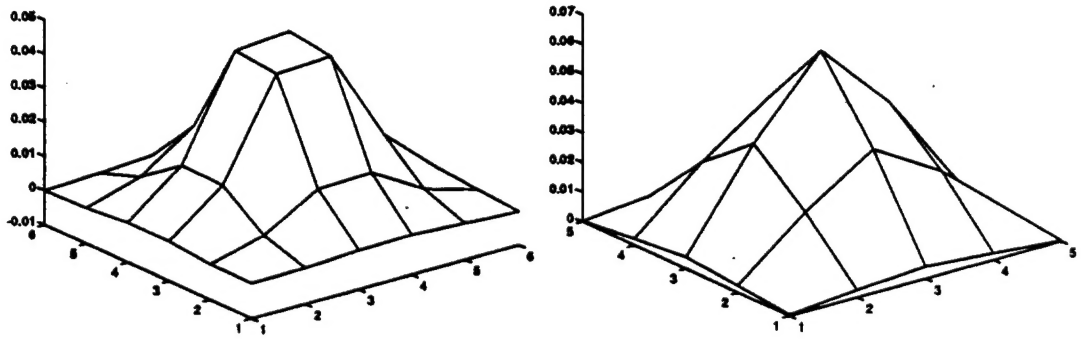

(a) (b)

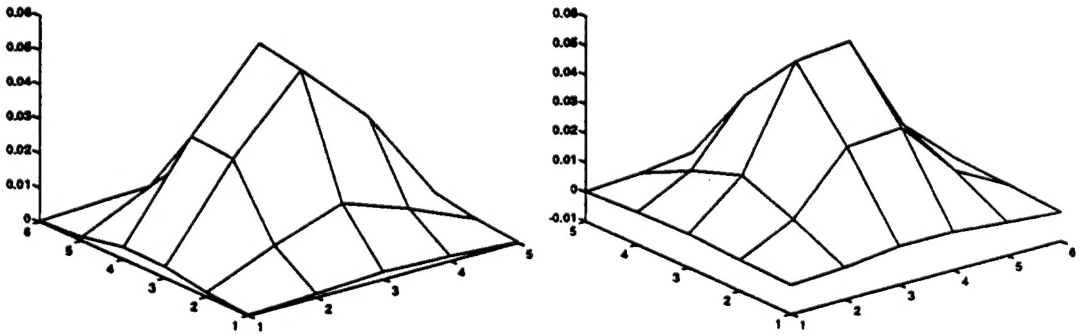

(c) (d)

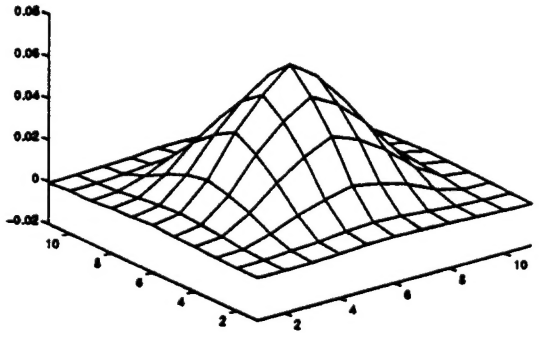

(e)

Figure 6: Observations: (a), (b), (c), (d) Four staggered blurred 2D signals, (e) interleaved observations.

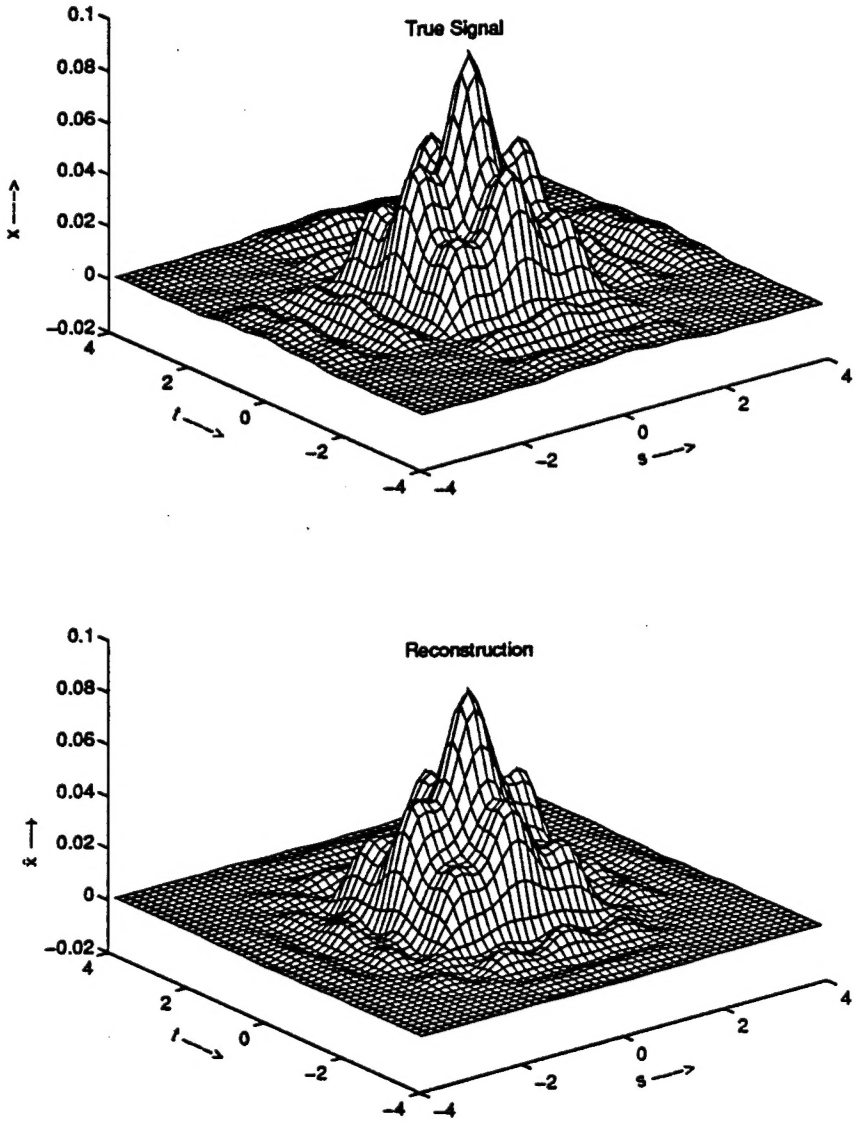

Figure 7: Signal, $x(t,s)$, and reconstruction, $\hat{x}(t,s)$.

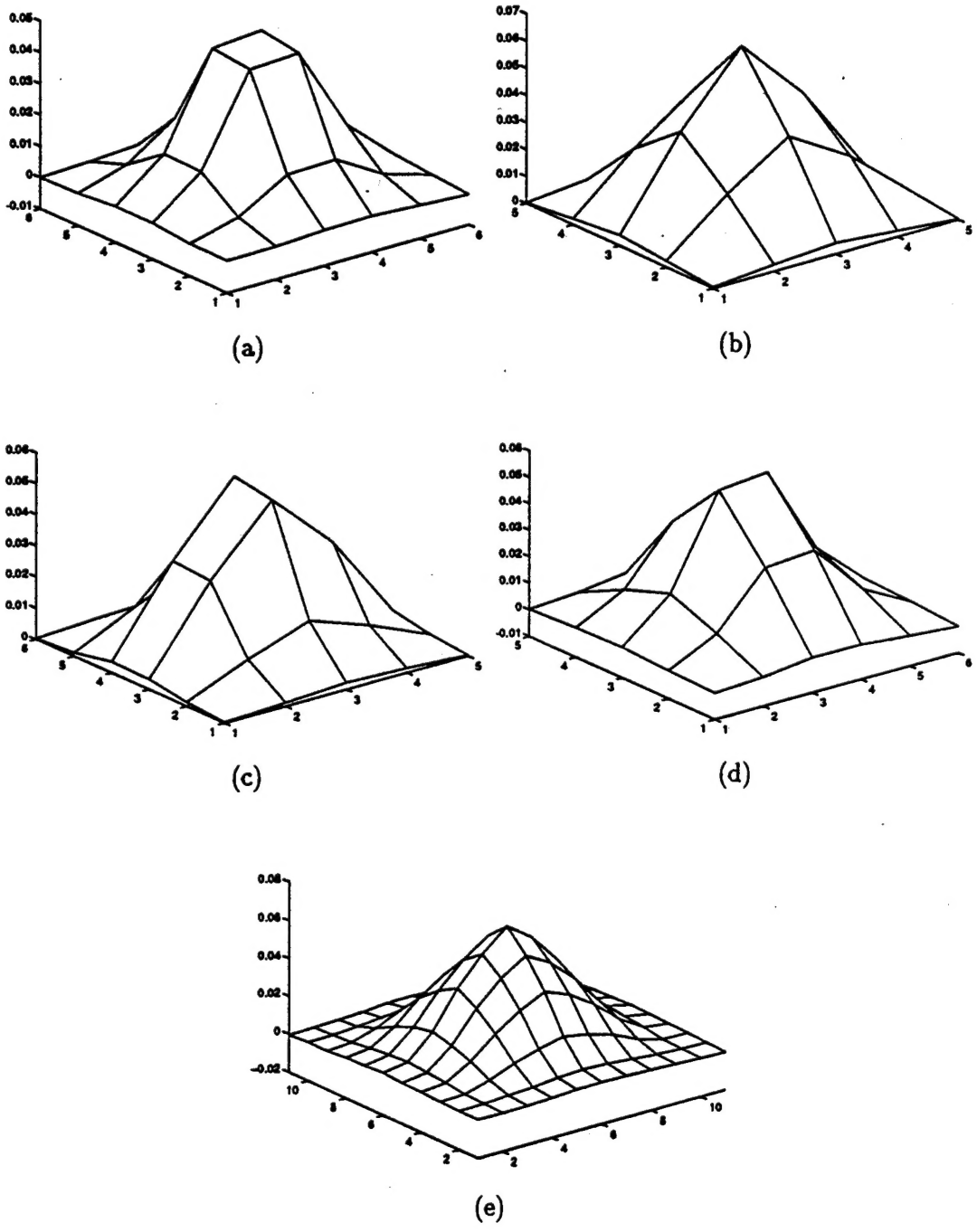

Figure 6: Observations: (a), (b), (c), (d) Four staggered blurred 2D signals, (e) interleaved observations.